Optimal Design of Modern Transformerless PV Inverter Topologies

Stefanos Saridakis, Eftichios Koutroulis, *Member, IEEE*, and Frede Blaabjerg, *Fellow, IEEE*

Abstract—The design optimization of H5, H6, neutral point clamped, active-neutral point clamped, and conergy-NPC transformerless photovoltaic (PV) inverters is presented in this paper. The components reliability in terms of the corresponding malfunctions, affecting the PV inverter maintenance cost during the operational lifetime period of the PV installation, is also considered in the optimization process. According to the results of the proposed design method, different optimal values of the PV inverter design variables are derived for each PV inverter topology and installation site. The H5, H6, neutral point clamped, active-neutral point clamped and conergy-NPC PV inverters designed using the proposed optimization process feature lower levelized cost of generated electricity and lifetime cost, longer mean time between failures and inject more PV-generated energy into the electric grid than their nonoptimized counterparts, thus maximizing the total economic benefit obtained during the operational time of the PV system.

Index Terms—DC/AC inverter, optimization, photovoltaic (PV) system, reliability, transformerless.

I. INTRODUCTION

THE modern grid-connected PV energy production systems widely employ transformerless photovoltaic (PV) dc/ac converters (inverters), since compared to the inverters using galvanic isolation they exhibit the advantages of lower cost, higher power density, and higher efficiency [1]–[3]. The block diagram of a grid-connected transformerless PV inverter is illustrated in Fig. 1. The PV array consists of PV modules connected in series and/or parallel [4], [5]. Typically, the power switches (e.g., IGBTs, SiC-based JFETs, etc.) of the power section of the PV inverter are controlled by a DSP- or FPGA-based microelectronic control unit according to pulse width modulation (PWM) techniques (e.g., sinusoidal PWM, space-vector PWM, hysteresis band control, etc.) [6]–[8]. A sinusoidal current with low harmonic content is injected into the electric grid by filtering the high-frequency harmonics of the PWM waveform produced at the output of the PV inverter power section. The use of *LCL*-type output filters, instead of the *L*- or *LC*-type filters, aims to increase the power density of the PV inverter [9].
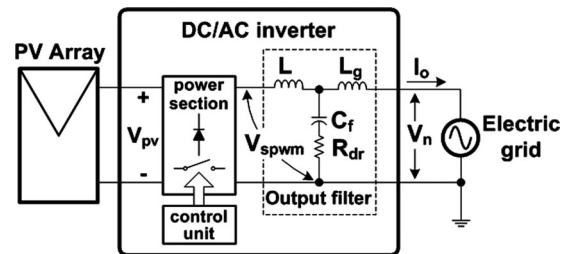
Fig. 1.   Block diagram of a transformerless PV inverter.

Many alternative topologies have been proposed during the last few years in order to build the power section of single- and three-phase transformerless PV inverters in grid-connected PV installations [10]–[19]. Among them, the H5, H6, and conergy-neutral point clamped (conergy-NPC) topologies have been integrated in commercially available grid-connected PV inverters. Also, the NPC and Active-NPC (ANPC) transformerless structures are widely used to build the power stage of PV inverters used in distributed generation systems, due to their low-leakage-current and high-efficiency features [20]. The H5, H6, NPC, ANPC, and conergy-NPC topologies are illustrated in Fig. 2. Compared to the H5 and H6 transformerless PV inverters, a higher dc input voltage is required for the operation of the NPC, ANPC, and conergy-NPC inverters.

In order to maximize the amount of energy injected into the electric grid and the total economic benefit achieved by a grid-connected PV installation during its operational lifetime period it is indispensable to maximize the reliability of the individual components and devices comprising the PV system [21], [22]. The reliability features are expressed in terms of indices such as the failure rate or the mean time between failures (MTBF) [23]. The design and production of PV power processing systems with high efficiency, high reliability and low cost features has been indicated in [24] as a major challenge. The PV inverters are typically designed according to iterative trial-and-error methods, which target to maximize the power conversion efficiency at nominal operating conditions or the "European Efficiency" of the PV inverter [19], [25]–[27]. The design optimization of transformerless PV inverters employing full-bridge, NPC, or ANPC topologies, has been analyzed in [20], [28], without, however, considering the reliability characteristics of the PV inverter. Also, various methods have been presented for the exploration and improvement of the PV inverters reliability performance, which are reviewed in [22]. However, these methods have the disadvantage that the concurrent impact of different critical design parameters, such as the PV inverter topology, component values, operational characteristics (e.g., maximum
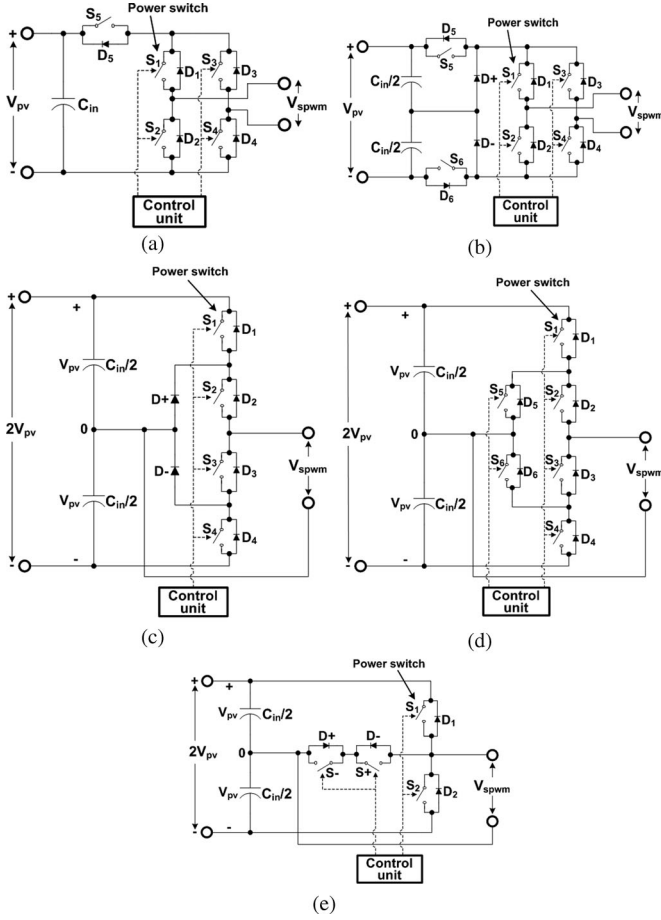
Fig. 2.   Topologies of the power section in transformerless single-phase PV inverters: (a) H5-inverter, (b) H6-inverter, (c) NPC, (d) ANPC, and (e) conergy-NPC.

switching frequency) and reliability performance, on the trade-off between the PV inverter manufacturing cost, maintenance cost, and total power losses, which affect the amount of energy injected into the electric grid by the PV inverter, is not considered during the PV inverter design process.

In this paper, the design technique including reliability, which was suited to full-bridge PV inverters in [22], is advanced in terms of the power-section topology, thus resulting in a new methodology for the optimal design of transformerless PV inverters based on the H5, H6, NPC, ANPC, and conergy-NPC structures. Using the proposed design process, the optimal values of components comprising the H5, H6, NPC, ANPC, and conergy-NPC PV inverters are calculated such that the PV inverter levelized cost of generated Electricity (LCOE) is minimized. The components reliability in terms of the corresponding malfunctions, which affect the PV inverter maintenance cost during the PV system operational lifetime period, as well as the limitations imposed by the electrical grid interconnection regulations and international standards, are also considered in the LCOE calculation. In contrast to the past-proposed approaches applied to design H5, H6, NPC, ANPC, and conergy-NPC PV inverters, the optimal design process presented in this paper has the advantage of taking into account the concurrent influences

of the meteorological conditions prevailing at the installation site, the PV inverter topology, as well as the cost, operational characteristics and reliability features of the components comprising the PV inverter, on both the PV inverter lifetime cost and total energy injected into the electric grid. The proposed design tool accommodates a systematic design flow based on conventional models and circuit-analysis techniques, which enables to calculate the optimal structure of H5, H6, NPC, ANPC, and conergy-NPC PV inverters among computationally complex alternatives, with minimum effort from the designer of the PV inverter.

This paper is organized as follows: the methodology for optimal design of transformerless PV inverters considering reliability is outlined in Section II; the modeling for optimization of H5, H6, NPC, ANPC, and conergy-NPC transformerless PV inverter topologies is analyzed in Section III, and the design optimization results are presented in Section IV. Finally, the topologies are compared in terms of their performance in various installation sites and conclusions are drawn.

II.   OPTIMAL DESIGN METHODOLOGY INCLUDING RELIABILITY

The proposed design optimization method calculates, for each of the H5, H6, NPC, ANPC, and conergy-NPC transformerless PV inverters, the optimal values of the switching frequency f_s(Hz) and the values of the components comprising the output filter, i.e., L, L_g, C_f, and R_{dr} in Fig. 1, such that the PV-inverter LCOE [29], LCOE (€/Wh), is minimized, while simultaneously the PV inverter specifications and the constraints imposed by the grid codes and international standards are satisfied like

$$\underset{\boldsymbol{X}}{\mathrm{minimize}}\{\mathrm{LCOE}(\boldsymbol{X})\}$$

subject to: design specifications and constraints are met   (1)

where

$$\mathrm{LCOE}(\boldsymbol{X}) = \frac{C_{\mathrm{inv}}(\boldsymbol{X})}{E_i(\boldsymbol{X})} \qquad (2)$$

with $C_{\mathrm{inv}}(\boldsymbol{X})$(€) being the present value of the PV inverter total cost during its operational lifetime period, $E_i(\boldsymbol{X})$(Wh) being the total energy injected into the electric grid by the PV inverter during its operational lifetime period, and $\boldsymbol{X} = [f_s|L|L_g|C_f]$ being the vector of the design variables.

The value of the LCL-filter damping resistor R_{dr} is calculated using the values of $\boldsymbol{X}$, as analyzed in [30]. The optimal value of the decision variables vector $\boldsymbol{X}$ is calculated using genetic algorithms (GAs), since they are capable to solve complex optimization problems with computational efficiency. A flowchart of the proposed design procedure, which is executed for each PV inverter topology, is illustrated in Fig. 3. Initially, the PV inverter designer provides as inputs the specifications of the PV inverter (e.g., nominal power, output voltage, etc.), the technical and economical characteristics of the components comprising the PV inverter, the operational characteristics of the PV array connected to the dc input of the PV inverter and the 1-h average values of the solar irradiation and ambient temperature conditions during the year at the PV inverter installation
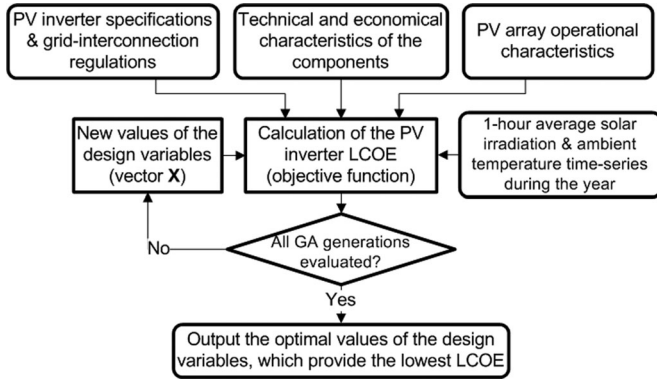
Fig. 3.   Flowchart of the proposed optimization process.

site. During the optimization process, multiple design vectors $\boldsymbol{X}$ composing the population of the GA process chromosomes, are progressively modified for a predefined number of generations. The LCOE objective function in (2) is calculated for each chromosome. The design vector $\boldsymbol{X}$ providing the lowest value of LCOE is comprised of the optimal values of the PV inverter design parameters.

In (1), the LCOE minimization is performed subject to the following constraints: 1) the ripple of the PV inverter output current is less than the maximum permissible limit, which is defined in the grid-interconnection regulations and/or standards (e.g., the IEEE-1547 standard); 2) the resonance-frequency, capacitance, and total inductance of the *LCL*-filter are constrained within the limits described in [30]; and 3) the value of the switching frequency f_s is limited by the maximum possible operating switching speed of the power switches and diodes composing the power section of the PV inverter $f_{s,\max}$(Hz) specified by their manufacturer, such that $f_s \leq f_{s,\max}$.

The present value of the PV inverter total cost, $C_{\mathrm{inv}}(\boldsymbol{X})$ in (2), is calculated as the sum of the PV inverter manufacturing cost, $C_t(\boldsymbol{X})$(€) and the present value of the total cost for maintaining the PV inverter during its operational lifetime period, $M_t(\boldsymbol{X})$(€):

$$C_{\mathrm{inv}}(\boldsymbol{X}) = C_t(\boldsymbol{X}) + M_t(\boldsymbol{X}). \tag{3}$$

The manufacturing cost C_t is equal to the sum of the costs of the individual components comprising the H5, H6, NPC, ANPC, and conergy-NPC PV inverters

$$C_t(\boldsymbol{X}) = c_{\mathrm{inv}} P_n + c_{\mathrm{hs}} + n_s c_s + n_d c_d + n_{\mathrm{cd}} c_{\mathrm{cd}}$$
$$+ c_i (L + L_g)\frac{P_n}{V_n} + c_c C_f + c_r R_{\mathrm{dr}} \cdot \mathrm{SF} \cdot P_{d,\max} \tag{4}$$

where c_{inv}(€/W) is the manufacturing cost of the PV inverter without including the cost of the heat sink, power switches, diodes, and *LCL*-filter components (e.g., control unit, printed circuit boards, integration, and housing etc.), c_{hs}(€) is the cost of the heat-sink, $n_s, n_d, n_{\mathrm{cd}}$ are the number of power switches, antiparallel diodes, and clamping diodes, respectively, contained in the PV inverter power section (for the H5, ANPC, and conergy-NPC topologies it holds that $n_{\mathrm{cd}} = 0$), $c_s, c_d, c_{\mathrm{cd}}$(€) are the cost of each power switch, antiparallel diode, and the clamping

diode, respectively, c_i[€/(H · A)] is the *LCL*-filter inductor cost per unit inductance and current, c_c(€/F) is the *LCL*-filter capacitor cost per unit capacitance, c_r[€/(Ω · W)] is the *LCL*-filter damping resistor cost per unit resistance and power, SF(%) is the oversizing factor of the damping resistor R_{dr}(see Fig. 1) and $P_{d,\max}$(W) is the maximum power dissipated on the damping resistor during operation.

The type and values of the individual components comprising the PV inverter determine the reliability performance of the PV inverter during its operational lifetime period, which, in turn, defines the present value of the PV inverter total maintenance cost, $M_t(X)$ in (3). In the proposed methodology, the value of M_t is calculated by reducing the PV inverter repair expenses occurring during each future year of operation, to the corresponding present value, as follows:

$$M_t(X) = \sum_{j=1}^{n} N_j(X) \cdot M_{\mathrm{inv}} \cdot \frac{(1+g)^j}{(1+d)^j} \tag{5}$$

where n is the number of years of PV system operational lifetime period, $N_j(X)$ is the average number of PV inverter failures which are expected to occur during the jth year of operation $(1 \leq j \leq n)$, M_{inv}(€) is the present value of the PV inverter repair cost, g(%) is the annual inflation rate, and d(%) is the annual discount rate.

The values of $N_j(X)$ in (5) are determined by the failure rate of the PV inverter, which in turn depends on the values of the individual components comprising the PV inverter and the stress factor applied to them (e.g., dc input voltage, ambient temperature, etc.) [31], as analyzed next. The total failure rate of the PV inverter, $\lambda_{\mathrm{inv}}(X)$ (number of failures/10^6 h) is a function of the design variables values X and it is calculated using the following equation:

$\lambda_{\mathrm{inv}}(X)$

$$= \frac{1}{\mathrm{MTBF}} = \lambda_{Cin}(C_{in}, \overline{V_{\mathrm{pv}}}, \overline{T_A}) + \sum_{i=1}^{n_s} \lambda_{\mathrm{ps},i}(\overline{T_{j\mathrm{ps},i}})$$
$$+ \sum_{i=1}^{n_d} \lambda_{d,i}(\overline{T_{jd,i}}) + \sum_{i=1}^{n_{cd}} \lambda_{cd,i}(\overline{T_{jcd,i}}) + \lambda_L(\overline{T_L}) + \lambda_{Lg}(\overline{T_{Lg}})$$
$$+ \lambda_{Cf}(C_f, \overline{V_{Cf}}, \overline{T_A}) + \lambda_{R_{\mathrm{dr}}}(\overline{P_{R_{\mathrm{dr}}}}, \overline{T_{R_{\mathrm{dr}}}}) + \lambda_c \tag{6}$$

where MTBF(h) is the mean time between failures of the PV inverter, $\lambda_{\mathrm{ps},i}, \lambda_{d,i}, \lambda_{\mathrm{cd},i}, \lambda_L, \lambda_{L_g}, \lambda_{C_f}$ and $\lambda_{R_{\mathrm{dr}}}$ (number of failures/10^6 hours) are the failure rates of the PV inverter power switches, free-wheeling diodes, clamping diodes, *LCL*-type output filter inductors L and L_g, capacitor C_f and damping resistor R_{dr}, respectively, λ_{Cin} is the total failure rate of the dc-link capacitor(s), λ_c is the total failure rate of the remaining components and subsystems comprising the PV inverter (e.g. digital circuits of the control unit, monitoring sensors, etc.), $\overline{T_A}$ is the weighted-average value of ambient temperature, $\overline{T_{j\mathrm{ps},i}}, \overline{T_{jd,i}}$, and $\overline{T_{j\mathrm{cd},i}}$ are the weighted-average values of the junction temperature of the power switches, free-wheeling diodes, and clamping diodes, respectively, and $\overline{V_{\mathrm{pv}}}, \overline{V_{Cf}}, \overline{P_{R_{\mathrm{dr}}}}, \overline{T_L}, \overline{T_{Lg}}$, and $\overline{T_{R_{\mathrm{dr}}}}$ are the weighted-average values of the PV inverter dc

input voltage (i.e., PV array output voltage), LCL-filter capacitor voltage, damping resistor power consumption, and operating temperature levels of the LCL-filter components (i.e. L, L_g, and R_{dr}), respectively.

The values of $\lambda_{\mathrm{ps},i}, \lambda_{d,i}, \lambda_{\mathrm{cd},i}, \lambda_L, \lambda_{Lg}, \lambda_{Cf}, \lambda_{R_{\mathrm{dr}}}$, and λ_{Cin} in (6) are calculated using the mathematical model of the PV inverter, the electrical specifications of the components used to build the PV inverter and the 1-h average solar irradiance and ambient temperature time-series during the year, according to the failure-rate models described in [31], [32]. The value of $\lambda_{\mathrm{inv}}(X)$ in (6) is calculated for each set of design variables values (i.e., vector X), which are produced during the evolution of the GA-based optimization process. The total failure rate $\lambda_{\mathrm{inv}}(X)$, determines the probability that the PV inverter will not operate properly, according to the exponential distribution [32]. Thus, the total number of failures that the PV inverter encounters during each year of operation is statistically variable. In the proposed methodology, in order to calculate the present value of the PV inverter total maintenance cost in (2) and (5), the average number of failures during each year of operation, $N_j(X)$ in (5), is calculated using the resulting value of $\lambda_{\mathrm{inv}}(X)$ and executing a Monte Carlo simulation with 10000 samples.

The total energy production of the PV inverter, E_i in (2), is calculated using the time series of the PV inverter power production during the PV system operational lifetime period, as follows:

$$E_i(X) = \sum_{y=1}^{n} \sum_{t=1}^{8760} P_o(t,y) \cdot \Delta t \qquad (7)$$

where $P_o(t,y)$ is the power injected into the electric grid by the PV inverter at hour t $(1 \leq t \leq 8760)$ of year y $(1 \leq y \leq n)$ and $\Delta t = 1$ h is the simulation time step.

The values of $P_o(t,y)$ in (7) are calculated according to the transformerless PV inverter modeling analyzed next.

III. MODELING OF TRANSFORMERLESS PV INVERTER TOPOLOGIES FOR OPTIMIZATION

With reference to the block diagram of transformerless PV inverters, which is illustrated in Fig. 1, the power injected into the electric grid by the PV inverter is calculated in the proposed methodology from a power-balance equation as follows:

$$P_o(t,y) = P_{\mathrm{pv}}(t,y) - P_{\mathrm{tot}}(t,y) \qquad (8)$$

where P_{pv} and P_{tot}(W) are the PV array output power and the PV inverter total power loss, respectively, at hour t $(1 \leq t \leq 8760)$ of year y $(1 \leq y \leq n)$.

Typically, the control unit of the PV inverter executes a maximum power point tracking (MPPT) process, such that the maximum possible power is produced by the PV array [33], [34]. The deterioration of the PV modules output power capacity during the operational lifetime period of the PV inverter affects the values of the stress factors applied to the PV inverter components and the values of the resulting failure rates in (6). Considering these parameters, the PV array output power, P_{pv}(W) in (8), is

calculated in the proposed methodology as follows:

$$P_{\mathrm{pv}}(t,y) = [1 - y \times r(y)] \cdot n_{\mathrm{mppt}} \cdot P_M(t) \qquad (9)$$

where y is the number of year of PV system operation $(1 \leq y \leq n)$, $r(\cdot)$ (%/year) is the annual reduction coefficient of the PV modules output power (if $y = 1$, then $r(y) = 0$, while for $1 < y \leq n$ its value is specified by the manufacturer of the PV modules), n_{mppt}(%) is the MPPT efficiency, which expresses the accuracy of the MPPT process executed by the control unit of the PV inverter (typically $n_{\mathrm{mppt}} > 99.7\%$) [35] and $P_M(t)$(W) is the power production at the maximum power point of the PV array during hour t $(1 \leq t \leq 8760)$.

The value of P_M in (9) is calculated according to the PV modules model analyzed in [36], using the time series of hourly values of solar irradiation and ambient temperature during the year, the electrical specifications of the PV modules and their configuration within the PV array (i.e., connection in series and parallel), that the designer of the PV inverter inputs in the proposed optimization procedure.

The total power loss of the PV inverter, P_{tot} in (8), is equal to the sum of the conduction and switching losses of the power semiconductors (i.e., power switches, free-wheeling diodes, and clamping diodes) comprising the power section of the PV inverter, P_{cond}(W) and P_{sw}(W), respectively, the power loss on the *LCL*-filter damping resistor P_d(W) the core and winding losses of the *LCL*-filter inductors, $P_{L,c}$(W), and $P_{L,r}$(W), respectively, and the power consumption of the control unit (due to the circuits of the SPWM modulator, sensors etc.), P_{cu}(W)

$$P_{\mathrm{tot}} = P_{\mathrm{cond}} + P_{\mathrm{sw}} + P_d + P_{L,c} + P_{L,r} + P_{\mathrm{cu}}. \qquad (10)$$

The values of P_d, $P_{L,c}$, and $P_{L,r}$ are calculated using the power loss models presented in [28], while the designer of the PV inverter provides the value of P_{cu}.

Initially, the PV inverter output current, $I_o(t,y)$(A), at hour t $(1 \leq t \leq 8760)$ of year y $(1 \leq y \leq n)$ is calculated by solving numerically the following power-balance equation:

$$P_{\mathrm{pv}}(t,y) = P_{\mathrm{tot}}(t,y) + V_n \cdot I_o(t,y) \qquad (11)$$

where V_n(V) is the nominal RMS value of the PV inverter output voltage.

In the proposed methodology, the power switches and diodes, which constitute the power section of the PV inverter, are modeled as voltage sources connected in series with resistors. Thus, the conduction power losses of each power switch and diode (either clamping or free-wheeling), P_{cond}(W), are given by

$$P_{\mathrm{cond}}(t,y) = V_d \cdot I_{\mathrm{avg}} + R_d \cdot I_{\mathrm{rms}}^2 \qquad (12)$$

where V_d(V) and R_d(Ω) are the power switch or diode forward voltage and resistance, respectively and I_{avg}, I_{rms}(A) are the average and RMS values, respectively, of the power switch or diode current.
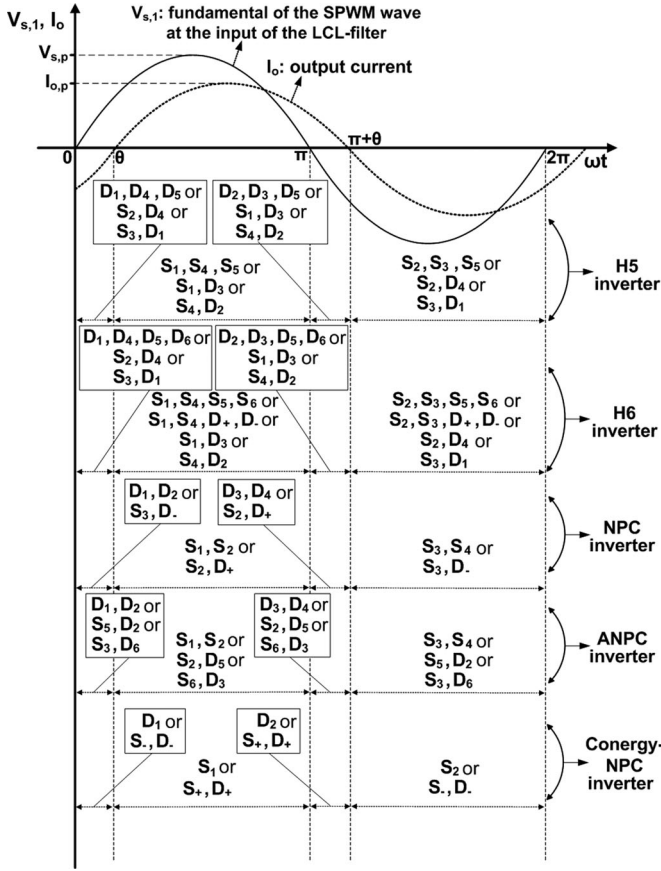
Fig. 4. Conducting devices in relation to the waveforms of $V_{s,1}$ and I_o for the H5, H6, NPC, ANPC, and conergy-NPC inverters.

The average and RMS values of the current of each power switch or diode are calculated as follows:

$$I_{\text{avg}} = \frac{1}{2\pi} \int_0^{2\pi} \sqrt{2} \cdot I_o(t,y) \cdot \sin(\omega t - \theta) \cdot f(\omega t) \cdot d\omega t \quad (13)$$

$$I_{\text{rms}} = \sqrt{\frac{1}{2\pi} \int_0^{2\pi} (\sqrt{2} \cdot I_o(t,y) \cdot \sin(\omega t - \theta))^2 \cdot f(\omega t) \cdot d\omega t} \quad (14)$$

where $f(\omega t)$ is the modulation function [37] of the corresponding power semiconductor, $I_o(t,y)$(A) is the RMS output current of the PV inverter at hour t $(1 \le t \le 8760)$ of year y $(1 \le y \le n)$ and θ $(°)$ is the phase difference between the PV inverter output current (i.e., I_o in Figs. 1 and 4) and the fundamental (i.e., $V_{s,1}$ in Fig. 4) of the SPWM voltage generated at the output terminals of the power section (i.e., V_{spwm} in Fig. 1).

The power semiconductors which conduct during each time interval of the output-current period of the H5, H6, NPC, ANPC, and conergy-NPC PV inverters, respectively, are also presented in Fig. 4. During the time intervals that a power semiconductor is not conducting, then the corresponding modulation function in (13) and (14) is set equal to zero [i.e., $f(\omega t) = 0$]. In the proposed methodology, the values of P_{cond} and P_{sw} in (10) are calculated by applying equations (11)–(14), which have been presented previously, for each of the H5, H6, NPC, ANPC,

TABLE I
CONDUCTION INTERVALS AND MODULATION FUNCTIONS OF THE H5 PV INVERTER

Power semiconductor	Conduction interval	Modulation function, $f(\omega t)$
S_1, S_4	$[\theta, \pi]$	$[1 + m_a \cdot \sin(\omega t)]/2$
	$[\pi, \pi + \theta]$	$[1 - m_a \cdot \sin(\omega t)]/2$
D_2, D_3	$[\theta, \pi]$	$[1 - m_a \cdot \sin(\omega t)]/2$
	$[\pi, \pi + \theta]$	$[1 + m_a \cdot \sin(\omega t)]/2$
S_5	$[\theta, \pi]$	$[1 + m_a \cdot \sin(\omega t)]/2$
	$[\pi + \theta, 2\pi]$	
D_5	$[0, \theta]$	$[1 - m_a \cdot \sin(\omega t)]/2$
	$[\pi, \pi + \theta]$	

and conergy-NPC topologies, as analyzed in the following paragraphs.

A. H5 PV inverter

The modulation functions of the H5-inverter power semiconductors, during each conduction interval presented in Fig. 4, are summarized in Table I as a function of the modulation index m_α of the PV inverter SPWM output voltage (i.e., V_{spwm} in Fig. 1). Considering the symmetrical operation of the H5 inverter topology and applying the modulation functions displayed in Table I in (13) and (14), it is derived that

$$I_{Si,\text{avg}} = I_{Sj,\text{avg}} = I_{S,\text{avg}}, \quad I_{Si,\text{rms}} = I_{Sj,\text{rms}} = I_{S,\text{rms}}$$

$$I_{Di,\text{avg}} = I_{Dj,\text{avg}} = I_{D,\text{avg}}, \quad I_{Di,\text{rms}} = I_{Dj,\text{rms}} = I_{D,\text{rms}}$$

$$(15)$$

where $i, j = 1, \dots, 4$.

Then, the total conduction loss, $P_{\text{cond}}(t,y)$, at hour t $(1 \le t \le 8760)$ of year y $(1 \le y \le n)$ of the H5-inverter is calculated as the sum of the conduction losses of the power switches and diodes comprising of the H5 inverter, using (12) and (15), as follows:

$$P_{\text{cond}}(t,y) = 4 \cdot (V_{s,\text{on}} I_{S,\text{avg}} + I_{S,\text{rms}}^2 R_{s,\text{on}}) + V_{s,\text{on}} I_{S5,\text{avg}}$$
$$+ I_{S5,\text{rms}}^2 R_{s,\text{on}} + 4 \cdot (V_d I_{D,\text{avg}} + I_{D,\text{rms}}^2 R_d)$$
$$+ V_d I_{D5,\text{avg}} + I_{D5,\text{rms}}^2 R_d. \quad (16)$$

The total switching energy, E(Joule) of the semiconductor devices in the H5 power section, which switch during the $0 \le \omega t \le \pi$ time interval depicted in Fig. 4, is calculated as the sum of the energy consumed by the power semiconductors during the corresponding turn-on and turn-off switching actions

$$E = \frac{V_{\text{pv}}(t,y) \cdot I_o(t,y) \cdot \sqrt{2} \cdot f_s}{V_t \cdot I_t \cdot 2\pi f} \cdot 2 \cdot (E_{\text{on}S1} + E_{\text{on}S4}$$
$$+ E_{\text{on}S5} + E_{\text{off}D1} + E_{\text{off}D4} + E_{\text{off}D5} + E_{\text{on}D1}$$
$$+ E_{\text{on}D4} + E_{\text{on}D5} + E_{\text{off}S1} + E_{\text{off}S4} + E_{\text{off}S5}) \quad (17)$$

where f_s(Hz) is the switching frequency, V_t(V), I_t(A) are the test voltage and current values, respectively, and $E_{\text{on}x_i}$, $E_{\text{off}x_i}$

TABLE II
CONDUCTION INTERVALS AND MODULATION FUNCTIONS
OF THE H6 PV INVERTER

Power semiconductor	Conduction interval	Modulation function, $f(\omega t)$
S_1, S_4	$[\theta, \pi]$	$[1 + m_a \cdot \sin(\omega t)]/2$
	$[\pi, \pi + \theta]$	$[1 - m_a \cdot \sin(\omega t)]/2$
D_2, D_3	$[\theta, \pi]$	$[1 - m_a \cdot \sin(\omega t)]/2$
	$[\pi, \pi + \theta]$	$[1 + m_a \cdot \sin(\omega t)]/2$
S_5, S_6	$[\theta, \pi]$	$[1 + m_a \cdot \sin(\omega t)]/2$
	$[\pi + \theta, 2\pi]$	
D_5, D_6	$[0, \theta]$	$[1 - m_a \cdot \sin(\omega t)]/2$
	$[\pi, \pi + \theta]$	
$D+, D-$	$[\theta, \pi]$	$[1 + m_a \cdot \sin(\omega t)]/2$
	$[\pi + \theta, 2\pi]$	

(Joule) are the turn-on and turn-off energy, respectively, of the power switch or free-wheeling diode x_i.

Since practically, power switches and diodes of the same operational characteristics are used to build the PV inverter, it holds that

$$E_{\mathrm{on}Si} = E_{\mathrm{on}Sj} = E_{\mathrm{on}T}, \quad E_{\mathrm{off}Si} = E_{\mathrm{off}Sj} = E_{\mathrm{off}T}$$

$$E_{\mathrm{on}Di} = E_{\mathrm{on}Dj} = E_{\mathrm{on}DT}, \quad E_{\mathrm{off}Di} = E_{\mathrm{off}Dj} = E_{\mathrm{off}DT} \quad (18)$$

where $i, j = 1 \ldots 5$, $E_{\mathrm{on}T}, E_{\mathrm{off}T}$ (Joule) are the power switch turn-on and turn-off energy and $E_{\mathrm{on}DT}, E_{\mathrm{off}DT}$ (Joule) are the free-wheeling diode turn-on and turn-off energy.

Due to the symmetrical operation of the H5-inverter topology, the total switching loss during the negative half-cycle of the output voltage period (i.e., during $[\pi - 2\pi]$) is equal to E in (17). Thus, the total switching losses of the H5-inverter, $P_{\mathrm{sw}}(t, y)$, at hour t ($1 \leq t \leq 8760$) of year y ($1 \leq y \leq n$) are calculated using (17) and (18), as follows:

$$P_{\mathrm{sw}}(t, y) = 2 \cdot f \cdot E = \frac{V_{\mathrm{pv}}(t, y) \cdot I_o(t, y) \cdot \sqrt{2} \cdot f_s}{\pi \cdot V_t \cdot I_t}$$
$$\cdot [6 \cdot (E_{\mathrm{on}T} + E_{\mathrm{on}DT}) + 6 \cdot (E_{\mathrm{off}T} + E_{\mathrm{off}DT})] \quad (19)$$

where f(Hz) is the frequency of the PV inverter output voltage.

B. H6 PV inverter

Due the symmetrical operation of the H6-inverter [see Fig. 2(b)] and applying the modulation functions displayed in Table II in (13) and (14), it results in

$$I_{Si,\mathrm{avg}} = I_{Sj,\mathrm{avg}} = I_{S,\mathrm{avg}}, \quad I_{Si,\mathrm{rms}} = I_{Sj,\mathrm{rms}} = I_{S,\mathrm{rms}}$$

$$I_{Di,\mathrm{avg}} = I_{Dj,\mathrm{avg}} = I_{D,\mathrm{avg}}, \quad I_{Di,\mathrm{rms}} = I_{Dj,\mathrm{rms}} = I_{D,\mathrm{rms}}$$

$$I_{S5,\mathrm{avg}} = I_{S6,\mathrm{avg}}, \quad I_{S5,\mathrm{rms}} = I_{S6,\mathrm{rms}}, \quad I_{D5,\mathrm{avg}} = I_{D6,\mathrm{avg}}$$

$$I_{D5,\mathrm{rms}} = I_{D6,\mathrm{rms}}, \quad I_{D+,\mathrm{avg}} = I_{D-,\mathrm{avg}}, \quad I_{D+,\mathrm{rms}} = I_{D-,\mathrm{rms}}$$
$$(20)$$

where $i, j = 1, ..., 4..$

The total conduction losses, $P_{\mathrm{cond}}(t, y)$, at hour t ($1 \leq t \leq 8760$) of year y ($1 \leq y \leq n$) of the power semiconductors used to build the H6 inverter are calculated using (12) and (20)

$$P_{\mathrm{cond}}(t, y) = 4 \cdot (V_{s,\mathrm{on}} I_{S,\mathrm{avg}} + I_{S,\mathrm{rms}}^2 R_{s,\mathrm{on}}) + 2$$
$$\cdot (V_{s,\mathrm{on}} I_{S5,\mathrm{avg}} + I_{S5,\mathrm{rms}}^2 R_{s,\mathrm{on}}) + 4$$
$$\cdot (V_d I_{D,\mathrm{avg}} + I_{D,\mathrm{rms}}^2 R_d)$$
$$+ 2 \cdot (V_d I_{D5,\mathrm{avg}} + I_{D5,\mathrm{rms}}^2 R_d) + 2$$
$$\cdot (V_d I_{D+,\mathrm{avg}} + I_{D+,\mathrm{rms}}^2 R_d). \quad (21)$$

Due to the symmetrical operation of the H6 inverter topology, the total switching losses for an H6 PV inverter, $P_{\mathrm{sw}}(t, y)$ in (10), are calculated by applying a similar procedure as that for the H5 topology described previously, resulting in

$$P_{\mathrm{sw}}(t, y) = 2 \cdot f \cdot E = \frac{V_{\mathrm{pv}}(t, y) \cdot I_o(t, y) \cdot \sqrt{2} \cdot f_s}{\pi \cdot V_t \cdot I_t}$$
$$\cdot [8 \cdot (E_{\mathrm{on}T} + E_{\mathrm{on}DT}) + 8 \cdot (E_{\mathrm{off}T} + E_{\mathrm{off}DT})$$
$$+ 4 \cdot (E_{\mathrm{on}D} + E_{\mathrm{off}D})]. \quad (22)$$

where $E_{\mathrm{on}D}$ and $E_{\mathrm{off}D}$ (Joule) are the clamping diode turn-on and turn-off energy, respectively.

C. NPC and ANPC PV inverters

The values of P_{cond} and P_{sw} in (8) for the NPC and ANPC PV inverters [see Fig. 2(c) and (d), respectively] are calculated using the power-loss models analyzed in detail in [20].

1) For the NPC PV inverter:

$$P_{\mathrm{cond}}(t, y) = 2 \cdot (V_{s,\mathrm{on}} I_{S1,\mathrm{avg}} + I_{S1,\mathrm{rms}}^2 R_{s,\mathrm{on}}$$
$$+ V_{s,\mathrm{on}} I_{S2,\mathrm{avg}} + I_{S2,\mathrm{rms}}^2 R_{s,\mathrm{on}})$$
$$+ 4 \cdot (V_d I_{D1,\mathrm{avg}} + I_{D1,\mathrm{rms}}^2 R_d)$$
$$+ 2 \cdot (V_d I_{D+,\mathrm{avg}} + I_{D+,\mathrm{rms}}^2 R_d) \quad (23)$$

$$P_{\mathrm{sw}}(t, y) = \frac{V_{\mathrm{pv}}(t, y) \cdot I_o(t, y) \cdot \sqrt{2} \cdot f_s}{2\pi \cdot V_t \cdot I_t}$$
$$\cdot [4 \cdot (E_{\mathrm{on}T} + E_{\mathrm{off}T}) + 2 \cdot (E_{\mathrm{on}D} + E_{\mathrm{off}D})$$
$$+ 2 \cdot (E_{\mathrm{on}DT} + E_{\mathrm{off}DT}) + 2 \cdot (E_{\mathrm{on},T}$$
$$+ E_{\mathrm{off},T} - E_{\mathrm{on},DT} - E_{\mathrm{off},DT}) \cdot \cos\theta]. \quad (24)$$

2) For the ANPC PV inverter:

$$P_{\mathrm{cond}}(t, y) = 2 \cdot (V_{s,\mathrm{on}} I_{S1,\mathrm{avg}} + I_{S1,\mathrm{rms}}^2 R_{s,\mathrm{on}}$$
$$+ V_{s,\mathrm{on}} I_{S2,\mathrm{avg}} + I_{S2,\mathrm{rms}}^2 R_{s,\mathrm{on}}$$
$$+ V_{s,\mathrm{on}} I_{S5,\mathrm{avg}} + I_{S5,\mathrm{rms}}^2 R_{s,\mathrm{on}})$$
$$+ 2 \cdot (V_d I_{D1,\mathrm{avg}} + I_{D1,\mathrm{rms}}^2 R_d$$
$$+ V_d I_{D2,\mathrm{avg}} + I_{D2,\mathrm{rms}}^2 R_d + V_d I_{D5,\mathrm{avg}}$$
$$+ I_{D5,\mathrm{rms}}^2 R_d) \quad (25)$$

TABLE III
CONDUCTION INTERVALS AND MODULATION FUNCTIONS OF THE
CONERGY-NPC PV INVERTER

Power semiconductor	Conduction interval	Modulation function, $f(\omega t)$
S_1	$[\theta, \pi]$	$m_a \cdot \sin(\omega t)$
D_1	$[0, \theta]$	$m_a \cdot \sin(\omega t)$
$S+$	$[\theta, \pi]$	$1 - m_a \cdot \sin(\omega t)$
	$[\pi, \pi+\theta]$	$1 + m_a \cdot \sin(\omega t)$
$D+$	$[\theta, \pi]$	$1 - m_a \cdot \sin(\omega t)$
	$[\pi, \pi+\theta]$	$1 + m_a \cdot \sin(\omega t)$

$$
\begin{aligned}
P_{\mathrm{sw}}(t,y) = {} & \frac{V_{\mathrm{pv}}(t,y) \cdot I_o(t,y) \cdot \sqrt{2} \cdot f_s}{2\pi \cdot V_t \cdot I_t} \\
& \cdot [6 \cdot (E_{\mathrm{on}T} + E_{\mathrm{on}DT}) \\
& + 12 \cdot (E_{\mathrm{off}T} + E_{\mathrm{off}DT}) + 2 \cdot (E_{\mathrm{on},T} + 2 \\
& \cdot E_{\mathrm{off},T} - E_{\mathrm{on},DT} - 2 \cdot E_{\mathrm{off},DT}) \cdot \cos\theta].
\end{aligned}
$$
(26)

D. Conergy-NPC PV inverter

The modulation functions of the power semiconductors comprising a conergy-NPC inverter [see Fig. 2(e)] are summarized in Table III. They have been derived by applying the on-state ratios of power semiconductors in SPWM 3-level inverters, which have been calculated in [38], for each of the power semiconductors in the corresponding conduction intervals depicted in Fig. 4. Considering the symmetrical operation of the conergy-NPC topology and applying the modulation functions displayed in Table III in (13) and (14), it results that

$$
\begin{aligned}
& I_{S1,\mathrm{avg}} = I_{S2,\mathrm{avg}} = I_{S,\mathrm{avg}}, \quad I_{S1,\mathrm{rms}} = I_{S2,\mathrm{rms}} = I_{S4,\mathrm{rms}} \\
& I_{D1,\mathrm{rms}} = I_{D2,\mathrm{rms}} = I_{D,\mathrm{rms}}, \quad I_{D1,\mathrm{avg}} = I_{D2,\mathrm{avg}} = I_{D,\mathrm{avg}} \\
& I_{S+,\mathrm{avg}} = I_{S-,\mathrm{avg}}, \quad I_{S+,\mathrm{rms}} = I_{S-,\mathrm{rms}} \\
& I_{D+,\mathrm{avg}} = I_{D-,\mathrm{avg}}, \quad I_{D+,\mathrm{rms}} = I_{D-,\mathrm{rms}}.
\end{aligned}
$$
(27)

The total conduction losses, $P_{\mathrm{cond}}(t,y)$, at hour t ($1 \leq t \leq 8760$) of year y ($1 \leq y \leq n$) of the power semiconductors employed in the conergy-NPC inverter are calculated using (12) and (27)

$$
\begin{aligned}
P_{\mathrm{cond}}(t,y) = {} & 2 \cdot (V_{s,\mathrm{on}} I_{S,\mathrm{avg}} + I_{S,\mathrm{rms}}^2 R_{s,\mathrm{on}}) \\
& + 2 \cdot (V_{s,\mathrm{on}} I_{S+,\mathrm{avg}} + I_{S+,\mathrm{rms}}^2 R_{s,\mathrm{on}}) \\
& + 2 \cdot (V_d I_{D,\mathrm{avg}} + I_{D,\mathrm{rms}}^2 R_d) \\
& + 2 \cdot (V_d I_{D+,\mathrm{avg}} + I_{D+,\mathrm{rms}}^2 R_d).
\end{aligned}
$$
(28)

The total switching energy, E_1 and E_2 (Joule) respectively, of the power semiconductor devices, which switch during the $0 \leq \omega t \leq \theta$ and $\theta \leq \omega t \leq \pi$ time intervals depicted in Fig. 4, are calculated as the sum of the energy consumed during the cor-

responding turn-on and turn-off switching actions, as follows:

$$
\begin{aligned}
E_1 = {} & \frac{V_{\mathrm{pv}}(t,y)/2}{V_t} \cdot \frac{I_o(t,y) \cdot \sqrt{2}}{I_t} \cdot \frac{f_s}{f} \cdot (E_{\mathrm{on}D1} + E_{\mathrm{off}S-} \\
& + E_{\mathrm{off}D-} + E_{\mathrm{on}S-} + E_{\mathrm{on}D-} + E_{\mathrm{off}D1}) \cdot \frac{1}{2\pi} \\
& \cdot \int_0^\theta \sin\lambda \, d\lambda
\end{aligned}
$$
(29)

$$
\begin{aligned}
E_2 = {} & \frac{V_{\mathrm{pv}}(t,y)/2}{V_t} \cdot \frac{I_o(t,y) \cdot \sqrt{2}}{I_t} \cdot \frac{f_s}{f} \cdot (E_{\mathrm{on}S1} + E_{\mathrm{off}S+} \\
& + E_{\mathrm{off}D+} + E_{\mathrm{off}S1} + E_{\mathrm{on}S+} + E_{\mathrm{on}fD+}) \cdot \frac{1}{2\pi} \\
& \cdot \int_\theta^\pi \sin\lambda \, d\lambda.
\end{aligned}
$$
(30)

The total switching losses of the conergy-NPC inverter, $P_{\mathrm{sw}}(t,y)$, at hour t ($1 \leq t \leq 8760$) of year y ($1 \leq y \leq n$) are calculated using (29) and (30), while simultaneously considering the symmetrical operation of the conergy-NPC inverter topology and that practically power switches and diodes of the same operational characteristics are used to build the PV inverter

$$
\begin{aligned}
P_{\mathrm{sw}}(t,y) = 2 \cdot f \cdot (E_1 + E_2) = {} & \frac{V_{\mathrm{pv}}(t,y) \cdot \sqrt{2} \cdot I_o(t,y)}{2\pi \cdot V_t \cdot I_t} \\
\cdot f_s \cdot [3(E_{\mathrm{on}T} + E_{\mathrm{on}DT}) & + 3(E_{\mathrm{off}T} + E_{\mathrm{off}DT}) \\
+ (E_{\mathrm{on},T} + E_{\mathrm{off},T} - E_{\mathrm{on},DT} & - E_{\mathrm{off},DT}) \cdot \cos\theta].
\end{aligned}
$$
(31)

IV. OPTIMAL SIZING RESULTS

The optimal design of single-phase, grid-connected PV inverters, which are based on the H5, H6, NPC, ANPC , and conergy-NPC transformerless topologies (Fig. 2) with $P_n = 2$ kW, $V_n = 220$ V, and $f = 50$ Hz, has been performed according to the optimization procedure described in Section II and using the models in Section III. The PV inverters under study comprise an LCL-type output filter and are connected to a PV array composed of PV modules with MPP power and voltage ratings, under standard test conditions (STC), equal to 175 W and 35.4 V, respectively. The service lifetime of the PV system is $n = 25$ years. During that time interval, the PV modules exhibit an annual reduction coefficient of their output power rating equal to $r(y) = 0.6\%$ in (9), as specified by their manufacturer.

The power section of all PV inverters consists of commercially available IGBT-type power switches with integrated freewheeling diodes. Discrete clamping diodes have been used in the H6- and NPC-based PV-inverters. The technical characteristics of the PV inverter components are based on the datasheet information provided by their manufacturers and they are presented in Table IV. According to the selling prices of the corresponding components in the international market, the economical characteristics of the PV inverter components are summarized in Table V. As discussed in Section II, the cost of integrating and housing the PV inverter subsystems has been included in the manufacturing cost, c_{inv}, which is displayed in Table V.

TABLE IV
TECHNICAL CHARACTERISTICS OF THE PV INVERTER COMPONENTS

power switches		power diodes		$E_{onT} + E_{onDT}$ (mJ)	$E_{offT} + E_{offDT}$ (mJ)	E_{onD} (mJ)	E_{offD} (mJ)	$f_{s,max}$ (kHz)	V_t (V)	I_t (A)
$V_{s,on}$ (V)	$R_{s,on}$ (mΩ)	V_d (V)	R_d (mΩ)							
0.75	83.3	0.87	120	0.09	0.11	$47.5 \cdot 10^{-9} \cdot V_{rr}$ V_{rr} : reverse voltage	0	30	400	6

TABLE V
ECONOMICAL CHARACTERISTICS OF THE PV INVERTER COMPONENTS

c_{inv} (€ / kW)	c_{hs} (€)	$c_s + c_d$ (€)	c_{cd} (€)	c_i (€ / H·A)	c_c (€ / F)	c_r (€ / (Ω·W))	M_{inv} (€)	g (%)	d (%)
327.8	27.2	1.5	0.91	832	$134 \cdot 10^3$	$3.6 \cdot 10^{-3}$	100.0	3.0	5.0

Fig. 5. Total cost of the optimized and nonoptimized H5, H6, NPC, ANPC, and conergy-NPC PV inverters for various installation sites in Europe.

A heat-sink with convection cooling and a $\theta_{ca} = 0.65\,°C/W$ thermal resistance has been selected such that the maximum junction temperature developed at the power semiconductors during the year is less than the 175 °C limit set by their manufacturer. The total failure rate of the PV inverter components, which are not included in the set of the PV inverter design variables, λ_c in (6), has been set equal to 17.2 failures/10^6 h [32], [39]. The maximum permissible output current ripple is limited to RF = 2% in order to conform to the IEEE-1547 standard. The damping resistor over-sizing factor has been set equal to SF = 110%. The control unit power consumption is $P_{cu} = 5$ W. The global minimum of the PV inverter LCOE (objective) function is calculated using a software program developed under the MATLAB platform. In this program, the GA optimization process has been implemented using the built-in genetic algorithm functions of the MATLAB global optimization toolbox and it is executed for 1000 generations, where each generation is comprised of a population of 40 chromosomes.

The optimal values of the PV inverter design variables (i.e. L, L_g, C_f, R_{dr} and f_s) and Levelized Cost Of the generated Electricity, LCOE$_{opt}$, which have been calculated using the proposed optimization process for the H5, H6, NPC, ANPC and conergy-NPC PV inverters installed in Athens (Greece), Oslo (Norway), Murcia (Spain) and Freiburg (Germany), respectively, are presented in Table VI. Different set of optimal values has been derived in each case, due to the different structure of the power semiconductors comprising each PV inverter topology and the different solar irradiation and ambient temperature conditions prevailing at each installation site, which affect the input voltage and power operating conditions of the PV inverters during their lifetime period. For the specific operational and economical characteristics of the components used to build the optimized PV inverters (see Tables IV and V) and depending on the PV inverter topology and installation location, the optimal value of the switching frequency, f_s in Table VI, has been calculated to be equal or close to the 30 kHz maximum limit of the power semiconductors considered, in order to minimize the contribution of the LCL-filter cost to the overall cost of the PV inverter [i.e., $C_{inv}(\boldsymbol{X})$ in (2) and (3)].

The LCOE values of the non-optimized H5, H6, NPC, ANPC and conergy-NPC PV inverters in each site, LCOE$_{n-o}$, are also presented in Table VI. The nonoptimized PV inverters are composed of the same semiconductors as the optimized PV inverters.
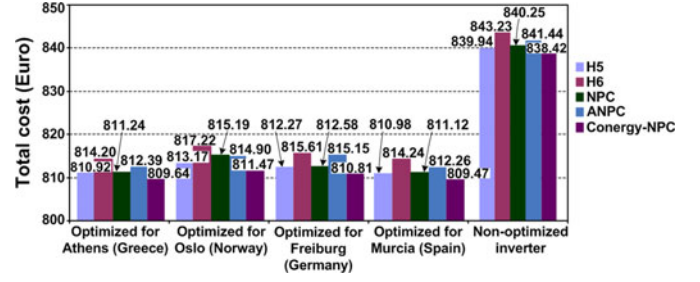
The *LCL* output filter of the nonoptimized PV inverters has been designed according to the methodology presented in [30] and it consists of: $L = 5.65$ mH, $L_g = 1.09$ mH, $C_f = 3.29$ μF, and $R_{dr} = 5.6$ Ω. The nonoptimized PV inverters operate with a switching frequency equal to $f_s = 8$ kHz, which is within the typical range of switching frequency values applied at power and voltage levels of this order [10], [19], [25]. Thus, in contrast to the procedure followed in the proposed methodology, the nonoptimized PV inverters have been designed using conventional techniques, without considering the manufacturing cost, energy production and number of failures in each installation site. The LCOE of the optimized PV inverters based on the H5, H6, NPC, ANPC and conergy-NPC topologies is lower by 7.02–9.05% compared to that of the corresponding nonoptimized PV inverter structures. At all installation sites, the best performance in terms of LCOE is achieved by the optimized conergy-NPC PV inverters. The optimal LCOE of the conergy-NPC inverters installed in Athens, Oslo, Murcia, and Freiburg, respectively, is lower than the optimal LCOE of the rest PV inverter topologies in the same installation sites by 0.44–1.67%, 0.45–1.72 %, 0.44–1.66%, and 0.45–1.70 %, respectively.

The lifetime cost, $C_{inv}(\boldsymbol{X})$ in (2) and (3), of the optimized and nonoptimized H5, H6, NPC, ANPC, and conergy-NPC PV inverters for various installation sites in Europe is depicted in Fig. 5. Compared to the nonoptimized PV inverters, the cost of the optimized H5, H6, NPC, ANPC, and conergy-NPC topologies is lower by 2.98–3.47%. At all installation sites, the minimum cost is achieved by the optimized conergy-NPC inverter and it is lower by 0.16–0.70% compared to that of the optimized PV inverters based on H5, H6, NPC, and ANPC topologies.

The total energy injected into the electric grid, $E_i(\boldsymbol{X})$ in (2) and (7), by the nonoptimized and optimized PV inverters in various installation sites in Europe is illustrated in Fig. 6(a) and (b), respectively. The energy injected into the electric grid by the optimized H5, H6, NPC, ANPC, and conergy-NPC PV inverters is higher compared to that of the corresponding nonoptimized structures in each installation site, by 3.83–6.35%. Among the optimized PV inverters, the conergy-NPC PV inverters achieve the maximum energy production in all installation sites. The PV-generated energy injected into the electric grid by the optimized conergy-NPC PV inverters is higher than that of the optimized PV inverters based on the H5, H6, NPC, and ANPC topologies by 0.08–0.76%.

TABLE VI
OPTIMAL VALUES OF THE DESIGN VARIABLES OF THE H5, H6, NPC, ANPC AND CONERGY-NPC PV INVERTERS AND THE LCOE
OF THE OPTIMIZED AND NONOPTIMIZED PV INVERTERS FOR VARIOUS INSTALLATION SITES IN EUROPE

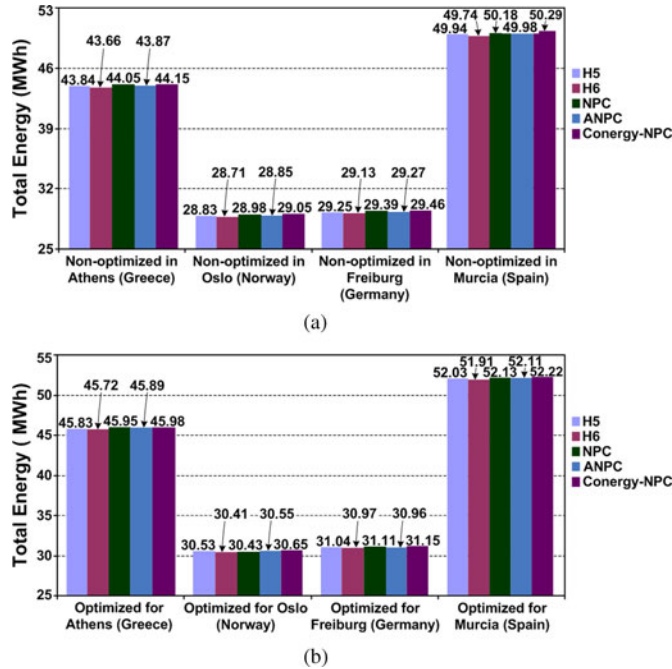|		L (mH)	L_g (µH)	C_f (µF)	R_{dr} (Ω)	f_s (kHz)	$LCOE_{opt}$ (€/MWh)	$LCOE_{n\text{-}o}$ (€/MWh)
Athens (Greece)	**H5**	2.825	43.232	5.919	2.682	30.00	17.692	19.159
	H6	2.825	51.907	4.920	3.219	30.00	17.810	19.313
	NPC	2.818	39.339	6.366	2.469	30.00	17.656	19.074
	ANPC	2.818	40.982	6.098	2.574	30.00	17.703	19.177
	Conergy-NPC	**2.852**	**42.270**	**5.876**	**2.662**	**30.00**	**17.597**	18.991
Oslo (Norway)	**H5**	3.119	39.439	6.216	2.503	29.95	26.633	29.133
	H6	3.214	36.592	6.455	2.368	29.95	26.870	29.371
	NPC	3.363	47.531	4.786	3.130	29.95	26.789	28.996
	ANPC	3.150	37.577	6.455	2.399	29.95	26.678	29.162
	Conergy-NPC	**3.091**	**46.174**	**5.978**	**2.759**	**29.95**	**26.478**	28.866
Murcia (Spain)	**H5**	2.825	37.680	6.577	2.378	30.00	15.586	16.820
	H6	2.825	42.945	5.755	2.711	30.00	15.685	16.954
	NPC	2.813	45.333	5.456	2.860	29.95	15.559	16.745
	ANPC	2.795	37.729	6.574	2.380	30.00	15.589	16.836
	Conergy-NPC	**2.825**	**38.189**	**6.470**	**2.413**	**30.00**	**15.502**	16.672
Freiburg (Germany)	**H5**	2.997	37.963	6.380	2.424	29.95	26.165	28.719
	H6	2.997	39.662	6.455	2.463	29.95	26.332	28.951
	NPC	2.997	37.546	6.455	2.397	29.95	26.117	28.586
	ANPC	3.180	37.606	6.455	2.400	29.95	26.330	28.747
	Conergy-NPC	**3.002**	**38.886**	**6.452**	**2.401**	**29.95**	**26.028**	28.458

Fig. 6.   Lifetime energy injected into the electric grid by the H5, H6, NPC, ANPC, and conergy-NPC PV inverters for various installation sites in Europe: (a) nonoptimized PV inverter and (b) optimized PV inverter.
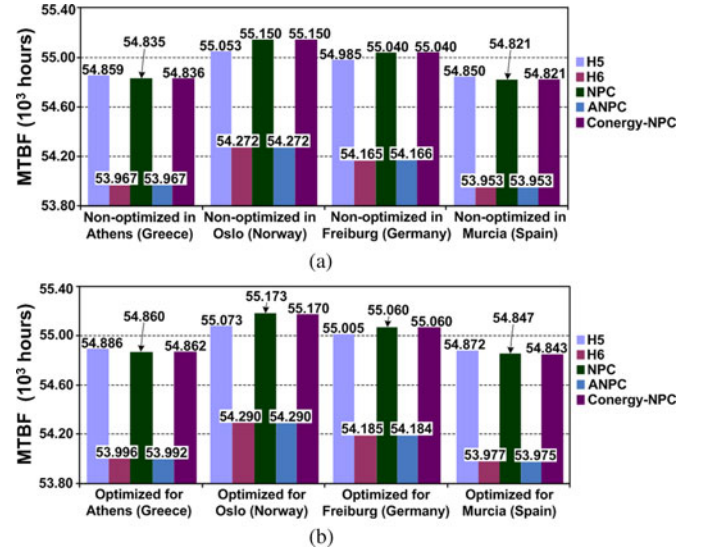

Fig. 7.   Mean time between failures (MTBF) of the H5, H6, NPC, ANPC, and conergy-NPC PV inverters for various installation sites in Europe: (a) nonoptimized PV inverter and (b) optimized PV inverter.

The MTBF of the nonoptimized and optimized H5, H6, NPC, ANPC, and conergy-NPC PV inverters for each installation site are presented in Fig. 7. It is observed that the H6 and ANPC topologies exhibit equivalent reliability performance. The same effect is observed for the NPC and conergy-NPC inverters. The MTBF of the H5 PV-inverters is close to that of the NPC and

conergy-NPC inverters. Also, for all PV inverter topologies under study, the PV inverters optimized for Murcia exhibit the worst performance in terms of MTBF, although, as illustrated in Table VI, they exhibit the minimum optimal LCOE. This is due to the increased values of the stress factors applied to the PV inverter components during operation, since the solar irradiation and ambient temperature are higher at this installation site. The MTBF values of the optimized H5, H6, NPC, ANPC, and conergy-NPC PV inverters are higher by 0.03–0.05% compared

to the MTBF of the corresponding nonoptimized PV inverter topologies. Among the PV inverter topologies examined, the optimized H5 inverters exhibit the best performance in terms of reliability in Athens and Murcia, where their MTBF is higher by 0.04–1.66% compared to that of the corresponding H6, NPC, ANPC, and conergy-NPC PV inverters which have been optimized for the same installation locations. Similarly, the MTBF of the optimized NPC and conergy-NPC inverters in Oslo and Freiburg is higher by 0.04–1.60% compared to the MTBF of the optimized H5, H6 and ANPC PV-inverters in these sites. As analyzed in Section II, the MTBF depends on the values of the components comprising the PV inverter and the stress factors applied at these components, which are determined by the meteorological conditions prevailing in each installation area. However, since the MTBF is calculated in (6) by weighting the values of the stress factors by the percentage of operating hours at each stress level, the impact of extreme individual values of the stress factors on the resulting MTBF is smoothed. Thus, depending on the installation location, the maximum deviation of the MTBF among the optimized PV inverters is 1.62–1.66%. At all installation sites, the H6 and ANPC PV inverters exhibit the lowest MTBF due to the larger number of components they consist of.

The optimal values of L, L_g, C_f, and f_s of optimized H5, H6, NPC, ANPC, and conergy-NPC PV inverters with $P_n = 10$ kW differ by 16.87–51.51%, 90.79–94.93%, 14.05–100.02%, and 266.25–275.00%, respectively, from the corresponding values of the nonoptimized PV inverter (also with $P_n = 10$ kW). In case that $P_n = 10$kW, the value of c_{inv} dominates in the PV inverter total cost [C_{inv} in (2) and (3)], thus reducing the sensitivity of LCOE with respect to the values of the design variables [i.e. vector X in (2)]. The resulting optimal LCOE values are lower than the LCOE of the nonoptimized PV inverters by 0.03–0.74%.

The convergence of the GA-based optimization procedure to the global minimum of the LCOE objective function has been verified by also applying an exhaustive-search method, which, however, requires more time in order to be completed than the GA process.

V. CONCLUSION

Among the transformerless PV inverter structures, the H5, H6, NPC, ANPC and conergy-NPC topologies are employed in commercially available grid-connected PV inverters and distributed generation systems. In this paper, a new methodology has been presented for calculating the optimal values of the components comprising the H5, H6, NPC, ANPC, and conergy-NPC PV inverters, such that the PV inverter LCOE is minimized. The components reliability in terms of the corresponding malfunctions, which affect the PV inverter maintenance cost during the operational lifetime period of the PV installation, is also considered in the optimization process. The proposed design method has the advantage of taking into account the concurrent influences of the PV inverter topology, the meteorological conditions prevailing at the installation site, as well as the PV inverter component cost, operational characteristics and relia-

bility features, on both the PV inverter lifetime cost and total energy production.

According to the design optimization results, the optimal values of the PV inverter design variables depend on the topology of the PV inverter power section (i.e. H5, H6, NPC, ANPC, and conergy-NPC) and the meteorological conditions at the installation site. Compared to the nonoptimized PV inverters, all PV inverter structures, which have been optimally designed using the proposed methodology, feature lower LCOE and lifetime cost, longer MTBF and inject more energy into the electric grid. Thus, by using the optimized PV inverters, the total economic benefit obtained during the lifetime period of the PV system is maximized.

REFERENCES

[1] M. C. Cavalcanti, K. C. de Oliveira, A. M. de Farias, F. A. S. Neves, G. M. S. Azevedo, and F. C. Camboim, "Modulation techniques to eliminate leakage currents in transformerless three-phase photovoltaic systems," *IEEE Trans. Ind. Electron.*, vol. 57, no. 4, pp. 1360–1368, Apr. 2010.

[2] O. Lopez, F. D. Freijedo, A. G. Yepes, P. Fernandez-Comesaa, J. Malvar, R. Teodorescu, and J. Doval-Gandoy, "Eliminating ground current in a transformerless photovoltaic application," *IEEE Trans. Energy Convers.*, vol. 25, no. 1, pp. 140–147, Mar. 2010.

[3] H. Patel and V. Agarwal, "A single-stage single-phase transformer-less doubly grounded grid-connected PV interface," *IEEE Trans. Energy Convers.*, vol. 24, no. 1, pp. 93–101, Mar. 2009.

[4] A. Mäki and S. Valkealahti, "Power losses in long string and parallel-connected short strings of series-connected silicon-based photovoltaic modules due to partial shading conditions," *IEEE Trans. Energy Convers.*, vol. 27, no. 1, pp. 173–183, Mar. 2012.

[5] M. E. Ropp and S. Gonzalez, "Development of a MATLAB/Simulink model of a single-phase grid-connected photovoltaic system," *IEEE Trans. Energy Convers.*, vol. 24, no. 1, pp. 195–202, Mar. 2009.

[6] R. Teodorescu, M. Liserre, and P. Rodríguez, *Grid Converters for Photovoltaic and Wind Power Systems*, 1st ed. New York, NY, USA: Wiley, 2011.

[7] L. Ma, X. Jin, T. Kerekes, M. Liserre, R. Teodorescu, and P. Rodriguez, "The PWM strategies of grid-connected distributed generation active NPC inverters," in *Proc. IEEE Energy Convers. Congr. Expo.*, 2009, pp. 920–927.

[8] H. Zang and X. Yang, "Simulation of two-level photovoltaic grid-connected system based on current control of hysteresis band," in *Proc. 2011 Asia-Pacific Power Energy Eng. Conf.*, 2011, pp. 1–4.

[9] G. Zeng, T. W. Rasmussen, and R. Teodorescu, "A novel optimized LCL-filter designing method for grid connected converter," in *Proc. 2nd IEEE Int. Symp. Power Electron. Distrib. Generation Syst.*, 2010, pp. 802–805.

[10] T. Kerekes, R. Teodorescu, P. Rodríguez, G. Vázquez, and E. Aldabas, "A new high-efficiency single-phase transformerless PV inverter topology," *IEEE Trans. Ind. Electron.*, vol. 58, no. 1, pp. 184–191, Jan. 2011.

[11] T. Kerekes, M. Liserre, R. Teodorescu, C. Klumpner, and M. Sumner, "Evaluation of three-phase transformerless photovoltaic inverter topologies," *IEEE Trans. Power Electron.*, vol. 24, no. 9, pp. 2202–2211, Sep. 2009.

[12] S. V. Araujo, P. Zacharias, and R. Mallwitz, "Highly efficient single-phase transformerless inverters for grid-connected photovoltaic systems," *IEEE Trans. Ind. Electron.*, vol. 57, no. 9, pp. 3118–3128, Sep. 2010.

[13] W. Yu, J.-S. Lai, H. Qian, and C. Hutchens, "High-Efficiency MOSFET inverter with H6-Type configuration for photovoltaic nonisolated AC-module applications," *IEEE Trans. Power Electron.*, vol. 26, no. 4, pp. 1253–1260, Apr. 2011.

[14] B. Yang, W. Li, Y. Gu, W. Cui, and X. He, "Improved transformerless inverter with common-mode leakage current elimination for a photovoltaic grid-connected power system," *IEEE Trans. Power Electron.*, vol. 27, no. 2, pp. 752–762, Feb. 2012.

[15] Z. Zhao, M. Xu, Q. Chen, J.-S. Lai, and Y. Cho, "Derivation, analysis, and implementation of a boost–buck converter-based high-efficiency PV inverter," *IEEE Trans. Power Electron.*, vol. 27, no. 3, pp. 1304–1313, Mar. 2012.

[16] H. Xiao and S. Xie, "Transformerless split-inductor neutral point clamped three-level PV grid-connected inverter," *IEEE Trans. Power Electron.*, vol. 27, no. 4, pp. 1799–1808, Apr. 2012.

[17] J.-M. Shen, H.-L. Jou, and J.-C. Wu, "Novel transformerless grid-connected power converter with negative grounding for photovoltaic generation system," *IEEE Trans. Power Electron.*, vol. 27, no. 4, pp. 1818–1829, Apr. 2012.

[18] A. Hasanzadeh, C. S. Edrington, and J. Leonard, "Reduced switch NPC-based transformerless PV inverter by developed switching pattern," in *Proc. 27th Annu. IEEE Appl. Power Electron. Conf. Expo.*, 2012, pp. 359–360.

[19] H. Xiao, S. Xie, Y. Chen, and R. Huang, "An Optimized Transformerless Photovoltaic Grid-Connected Inverter," *IEEE Trans. Ind. Electron.*, vol. 58, no. 5, pp. 1887–1895, May 2011.

[20] S. Saridakis, E. Koutroulis, and F. Blaabjerg, "Optimal design of NPC and Active-NPC transformerless PV inverters," in *Proc. 3rd IEEE Int. Symp. Power Electron. Distrib. Generation Syst.*, 2012, pp. 106–113.

[21] P. Zhang, Y. Wang, W. Xiao, and W. Li, "Reliability evaluation of grid-connected photovoltaic power systems," *IEEE Trans. Sustainable Energy*, vol. 3, no. 3, pp. 379–389, Jul. 2012.

[22] E. Koutroulis and F. Blaabjerg, "Design optimization of transformerless grid-connected PV inverters including reliability," *IEEE Trans. Power Electron.*, vol. 28, no. 1, pp. 325–335, 2013.

[23] F. Chan and H. Calleja, "Reliability estimation of three single-phase topologies in grid-connected PV systems," *IEEE Trans. Ind. Electron.*, vol. 58, no. 7, pp. 2683–2689, 2011.

[24] G. Petrone, G. Spagnuolo, R. Teodorescu, M. Veerachary, and M. Vitelli, "Reliability issues in photovoltaic power processing systems," *IEEE Trans. Ind. Electron.*, vol. 55, no. 7, pp. 2569–2580, Jul. 2008.

[25] R. Gonzalez, J. Lopez, P. Sanchis, and L. Marroyo, "Transformerless inverter for single-phase photovoltaic systems," *IEEE Trans. Power Electron.*, vol. 22, no. 2, pp. 693–697, Mar. 2007.

[26] A. C. Nanakos, E. C. Tatakis, and N. P. Papanikolaou, "A weighted-efficiency-oriented design methodology of flyback inverter for ac photovoltaic modules," *IEEE Trans. Power Electron.*, vol. 27, no. 7, pp. 3221–3233, Jul. 2012.

[27] T. Kerekes, R. Teodorescu, P. Rodríguez, G. Vázquez, and E. Aldabas, "A new high-efficiency single-phase transformerless PV inverter topology," *IEEE Trans. Ind. Electron.*, vol. 58, no. 1, pp. 184–191, Jan. 2011.

[28] E. Koutroulis and F. Blaabjerg, "Methodology for the optimal design of transformerless grid-connected PV inverters," *IET Power Electron.*, vol. 5, no. 8, pp. 1491–1499, 2012.

[29] M. Campbell, J. Blunden, E. Smeloff, and P. Aschenbrenner, "Minimizing utility-scale PV power plant LCOE through the use of high capacity factor configurations," in *Proc. 34th IEEE Photovoltaic Spec. Conf.*, 2009, pp. 421–426.

[30] M. Liserre, F. Blaabjerg, and S. Hansen, "Design and control of an LCL-filter-based three-phase active rectifier," *IEEE Trans. Ind. Appl.*, vol. 41, no. 5, pp. 1281–1291, Sep. 2005.

[31] *Reliability Prediction of Electronic Equipment*, Military Handbook 217-F, Department of Defense, USA, 1991.

[32] A. Ristow, M. Begovic, A. Pregelj, and A. Rohatgi, "Development of a methodology for improving photovoltaic inverter reliability," *IEEE Trans. Ind. Electron.*, vol. 55, no. 7, pp. 2581–2592, July 2008.

[33] H. Patel and V. Agarwal, "MPPT scheme for a PV-Fed single-phase single-stage grid-connected inverter operating in CCM with only one current sensor," *IEEE Trans. Energy Convers.*, vol. 24, no. 1, pp. 256–263, Mar. 2009.

[34] E. Koutroulis and F. Blaabjerg, "A new technique for tracking the global maximum power point of PV arrays operating under partial-shading conditions," *IEEE J. Photovoltaics*, vol. 2, no. 2, pp. 184–190, Apr. 2012.

[35] S. Jiang, D. Cao, Y. Li, and F. Peng, "Grid-Connected boost-half-bridge photovoltaic micro inverter system using repetitive current control and maximum power point tracking," *IEEE Trans. Power Electron.*, vol. 27, no. 11, pp. 4711–4722, Nov. 2012.

[36] E. Lorenzo, *Solar Electricity—Engineering of Photovoltaic Systems*, 1st ed. Sevilla, Spain: Progensa, 1994, pp. 87–99.

[37] D. Floricau, G. Gateau, A. Leredde, and R. Teodorescu, "The efficiency of three-level Active NPC converter for different PWM strategies," in *Proc. 13th Eur. Conf. Power Electron. Appl.*, 2009, pp. 1–9.

[38] T. J. Kim, D. W. Kang, Y. H. Lee, and D. S. Hyun, "The analysis of conduction and switching losses in multi-level inverter system," in *Proc. IEEE 32nd Annu. Power Electron. Spec. Conf.*, 2001, vol. 3, pp. 1363–1368.

[39] M. Aten, G. Towers, C. Whitley, P. Wheeler, J. Clare, and K. Bradley, "Reliability comparison of matrix and other converter topologies," *IEEE Trans. Aerosp. Electron. Syst.*, vol. 42, no. 3, pp. 867–875, Jul. 2006.

Stefanos Saridakis was born in Heraklion, Greece, in 1980. He received the B.Sc. degree in electrical engineering from the Technological Educational Institute of Crete, Heraklion, Greece, in 2004, and the Diploma in electrical and computer engineering from the Democritus University of Thrace, Xanthi, Greece, in 2011. He is currently working toward the M.Sc. degree from the Department of Electronic and Computer Engineering, the Technical University of Crete, Chania, Greece.

His research interests include power electronics for renewable energy sources, electric machines, and high-voltage direct-current power systems.

Eftichios Koutroulis (M'10) was born in Chania, Greece, in 1973. He received the B.Sc. and M.Sc. degrees from the Department of Electronic and Computer Engineering, the Technical University of Crete, Chania, Greece, in 1996 and 1999, respectively, and the Ph.D. degree in the area of power electronics and Renewable Energy Sources (RES) in 2002.

He is currently an Assistant Professor at the Department of Electronic and Computer Engineering of the Technical University of Crete. His research interests include power electronics (dc/ac inverters, dc/dc converters), the development of microelectronic energy management systems for RES and the design of photovoltaic and wind energy conversion systems.

Frede Blaabjerg (F'03) received the Ph.D. degree from the Aalborg University, Aalborg, Denmark, in 1992.

He was employed at ABB-Scandia, Randers, from 1987–1988. He became an Assistant Professor at Aalborg University, Aalborg, Denmark in 1992, an Associate Professor in 1996 and a Full Professor in power electronics and drives in 1998. He has been a part-time Research Leader at Research Center Risoe in wind turbines. During 2006—2010, he was the Dean of the faculty of Engineering, Science, and Medicine and became a Visiting Professor at Zhejiang University, Zhejiang, China in 2009. His research areas are in power electronics and its applications like in wind turbines, PV systems, and adjustable speed drives.

He has been an Editor-in-Chief of the IEEE TRANSACTIONS ON POWER ELECTRONICS from 2006—to 2012. He was a Distinguished Lecturer for the IEEE Power Electronics Society 2005–2007 and for IEEE Industry Applications Society from 2010–2011. He has been the Chairman of EPE'2007 and PEDG'2012—both held in Aalborg. He received the 1995 Angelos Award for his contribution in modulation technique and the Annual Teacher prize at Aalborg University. In 1998, he received the Outstanding Young Power Electronics Engineer Award from the IEEE Power Electronics Society. He has received thirteen IEEE Prize paper awards and another prize paper award at PELINCEC Poland 2005. He received the IEEE PELS Distinguished Service Award in 2009 and the EPE-PEMC 2010 Council award. Finally he has received a number of major research awards in Denmark.